Electronic structure and thermodynamic properties of the Heusler alloys $Fe_2Ti_{1-x}V_xSn$

A. Ślebarski,[1] J. Deniszczyk,[2] W. Borgieł,[1] A. Jezierski,[3] M. Swatek,[1] A. Winiarska,[1] M. B. Maple,[4] and W. M. Yuhasz[4]
[1]*Institute of Physics, University of Silesia, 40-007 Katowice, Poland*
[2]*Institute of Physics and Chemistry of Metals, University of Silesia, 40-007 Katowice, Poland*
[3]*Institute of Molecular Physics, Polish Academy of Sciences, 60-179 Poznań, Poland*
[4]*Department of Physics and Institute for Pure and Applied Physical Sciences, University of California, San Diego, La Jolla, California 92093-0360, USA*

(Received 23 July 2003; revised manuscript received 11 December 2003; published 30 April 2004)

The aim of this work is to investigate electronic structure, magnetic properties, and electrical resistivity of the $Fe_2Ti_{1-x}V_xSn$ Heusler alloys. We report x-ray photoelectron valence-band spectra and compare the results with those obtained from the self-consistent tight-binding linearized muffin-tin orbital method. The changes in electronic and magnetic structure of the $Fe_2Ti_{1-x}V_xSn$ alloys were also investigated by means of the Korringa-Kohn-Rostocker Green's-function method in the coherent potential approximation. Numerical calculations yield the magnetic ground state for the $Fe_2Ti_{1-x}V_xSn$ alloys, when $x \geqslant 0.2$ in agreement with Slater-Pauling behavior. The band-structure calculations give a narrow peak in the density of states located in the energy gap near the Fermi level which is attributed to Fe antisite defects. The numerical calculations are in agreement with the experimental results recently obtained from infrared investigations of Fe_2TiSn. We also report electrical resistivity calculations using a Falicov-Kimball model. Many-body calculations have shown that the narrow *d* band originating from the Fe impurity atoms is responsible for the unusual temperature dependencies of the physical properties of the $Fe_2Ti_{1-x}V_xSn$ alloys.

DOI: 10.1103/PhysRevB.69.155118 PACS number(s): 71.20.Be, 71.10.Hf, 71.27.+a, 75.20.Hr

I. INTRODUCTION

Fe_2TiSn belongs to a group of materials commonly referred to as Heusler alloys with the formula X_2YZ, where X and Y are two different transition metals and Z is a nonmagnetic element. Heusler alloys[1] have attracted great interest during the last 100 years due to their interesting and diverse magnetic properties such as itinerant and localized magnetism, Pauli paramagnetism or heavy-fermion (HF) behavior (e.g., Refs. 2–7). Two members of this family Fe_2VAl (Ref. 8) and Fe_2TiSn (Ref. 7) have recently attracted a lot of attention in connection with possible *d*-electron heavy-fermion behavior, where the resistivity displays an anomalous temperature dependence, and specific-heat measurements reveal an upturn in $C(T)/T$ resembling that of conventional *f*-electron HF compounds. However, band-structure calculations yield only a minor mass renormalization.[9–11] An infrared (IR) study reported recently for Fe_2VAl (Ref. 12) and Fe_2TiSn (Ref. 13) also finds no characteristic features of the HF state in these compounds. In contrast, the mass enhancement evident in the C/T upturn is still indicative of heavy-fermion-like behavior. The effective mass obtained for Fe_2TiSn corresponding to the value of the electronic specific heat γ is ~ 40 times the free-electron mass.

Fe_2TiSn is an excellent example of a Heusler-type alloy, in which the local environment profoundly influences the magnetic and electrical transport properties. The linearized muffin-tin orbital (LMTO) calculations[7] yield a nonmagnetic ground state and a pseudogap at the Fermi level ϵ_F, while the local disorder leads to weak ferromagnetism which destroys the gap at ϵ_F.[7] To better understand the influence of the magnetic ground state on the physical properties of Fe_2TiSn at ϵ_F, we present an investigation of the low-concentration antisite defects in Fe_2TiSn and $Fe_2Ti_{1-x}V_xSn$ alloys. Heusler alloys follow the well-known Slater-Pauling behavior for the binary transition metal alloys.[14] In such a picture the total spin moment M scales with the total number of valence electrons Z. For the Heusler alloys $M = Z - 24$.[15] In this simple picture, one expects $M = 0$ for Fe_2TiSn, while $M \neq 0$ for Fe_2VSn. Indeed, Fe_2VSn is known to be a ferromagnet with Curie temperature $T_C = 200$ K and $M = 1.32\ \mu_B$ per formula unit.[16]

The aim of this work is to investigate the electronic structure, electrical resistivity, and magnetic properties of $Fe_2Ti_{1-x}V_xSn$. Our band-structure calculations are in agreement with infrared and optical spectroscopy results and suggest an interband transition which can be interpreted as excitation across a pseudogap in the density of states (DOS) at ϵ_F.

II. EXPERIMENTAL DETAILS

Polycrystalline samples of $Fe_2Ti_{1-x}V_xSn$ have been prepared by arc melting the constituent elements (Fe 99.99%, Ti 99.99%, V 99.99%, Sn 99.999% in purity) on a water cooled copper hearth in a high-purity argon atmosphere with a Zr getter. Each sample was remelted several times to promote homogeneity and annealed at 800 °C for 2 weeks. The samples were carefully examined by x-ray-diffraction analysis and found to be single phase.

The dc magnetization was measured using a commercial superconducting quantum interference device magnetometer from 1.8 K to 400 K in magnetic fields up to 5 T.

Electrical resistivity measurements were made using a standard four-wire technique.

The XPS (x-ray photoelectron spectroscopy) spectra were obtained with monochromatized Al K_α radiation at room

temperature using a PHI 5700 ESCA spectrometer. The spectra were measured immediately after cleaving the sample in a vacuum of 10^{-10} Torr. The spectra were calibrated according to Ref. 17. Binding energies were referenced to the Fermi level ($\epsilon_F = 0$).

The electronic structure of the ordered compounds was studied by the all-electron self-consistent (LMTO) method and the calculations were performed using the TB LMTO-4.7 code.[18] To test the reliability of the approximate TB LMTO results and to investigate the effect of the Coulomb correlation interaction within the Fe-3d band states, the electronic structure of the stoichiometric Fe_2TiSn was also studied using the general potential (full potential) linear augmented plane-wave (FP-LAPW) method. The calculations were performed using the WIEN2K code.[19]

In the approximate TB-LMTO method the crystal potential is treated within the atomic sphere shape approximation (ASA)[20] with overlapping Wigner-Seitz (W-S) spheres centered at atomic positions. The values of the W-S sphere radii were determined in such a way that the sum of all atomic sphere volumes is equal to the volume of the unit cell. While in the FP-LAPW approach no such shape approximation is used and the crystal potential is expanded into spherical (lattice) harmonics within the muffin-tin (MT) atomic spheres and into plain waves outside MT spheres. The MT spheres of radii 2.2 and 2.3 a.u. were assumed for transition metal (Fe, Ti) and Sn atoms, respectively. All electronic structure calculations were performed using the experimental lattice parameters.

In both methods the local spin density approximation (LSDA) for the exchange-correlation (XC) potential was employed. In the TB-LMTO calculations the XC potential was assumed to be of the form proposed by von Barth-Hedin,[21] and Langreth-Mehl-Hu (LMH) generalized gradient corrections were included.[22] The FP-LAPW calculations were performed with the use of the gradient corrected LSD XC potential in the form developed by Perdew, Burke, and Ernzerhof (PBE).[23] The electronic structure of Fe_2TiSn was studied by means of FP-LAPW with the use of the PBE XC potential, corrected according to the LSDA+U method[24] to account for the Hubbard correlation interaction within the 3d-band states. The LSDA+U XC potential was implemented for the 3d orbitals of Fe atoms with values for Coulomb (U) and exchange (J) parameters equal to 1.2 eV and 0.73 eV, respectively (Ref. 25).

The TB-LMTO calculations of Fe_2TiSn were performed for 413 $\vec{k}$ points in the irreducible Brillouin zone (IBZ) with the total energy error of about 0.1 mRy. In the TB-LMTO semirelativistic calculations, we considered the spd atomic orbitals and the downfolded f states, while the 4d Sn electrons were treated as core states. Within the FP-LAPW calculations 500 ($7\times7\times7$) $\vec{k}$ points in the Brillouin zone were assumed (20 $\vec{k}$ vectors in IBZ). The $\vec{k}$ vectors together with a $R_{mt}\times K_{max}$ parameter of 9.0 result in a total energy error of 0.1 mRy. The basis set used in the FP-LAPW calculations included over 450 functions per unit cell. The local orbitals,[26] sp type for Fe, Ti, and spd type for Sn, were added in order to correct for linearization errors.

The numerical calculations of the electronic density of states of off-stoichiometric Fe_2TiSn with antisite (AS) defects were performed for a supercell $Fe_{16}Ti_8Sn_8$, which contained eight Fe_2TiSn formula units. We analyzed two different situations: (i) an excess of Fe atoms occupying the Ti atomic positions of the off-stoichiometric $Fe_{17}Ti_7Sn_8$ ($Fe_{21}Ti_9Sn_{10}$) sample, (ii) Fe and Ti atoms at antisite atomic positions ($Fe_{AS}\leftrightarrow Ti_{AS}$) in $[Fe_{15}Ti_{AS}][Ti_7Fe_{AS}]Sn_8$. In both situations, one lattice defect occurs per eight unit cells. The TB-LMTO calculations for ordered $Fe_2Ti_{1-x}V_xSn$ structures were performed for concentrations $x = 0.25$, 0.5, and 0.75 using a supercell with four underlying $L2_1$ unit cells.

Changes in the electronic and magnetic structure of $Fe_2Ti_{1-x}V_xSn$ alloys were investigated by means of the Korringa-Kohn-Rostoker Green's-function (KKR-GF) method[27] linked to the coherent potential approximation (CPA) alloy theory[28,29] using an exchange-correlation potential proposed by Vosko, Wolk, and Nusair.[30] The calculations have been spin polarized and all relativistic effects have been taken into account. The investigations were performed using the Munich SPR-KKR package (version 2.1) of Ebert *et al.* (Ref. 31).

III. RESULTS AND DISCUSSION

A. Structural properties

Listed in Table I are the experimentally obtained lattice parameters for $Fe_2Ti_{1-x}V_xSn$ alloys assuming an $L2_1$ cubic structure. A more detailed analysis of the x-ray diffraction data, in which the crystal structure of $Fe_2Ti_{1-x}V_xSn$ for $x < 0.5$ was refined with the Rietveld method, revealed the presence of crystallographic disorder. However, the shape of the reflections do not agree well with calculations, particularly in the 2θ range of the tail of each line which we have attributed to small distortions of the lattice resulting from atomic disorder.

The observed and calculated x-ray-diffraction intensities for the cubic structure (symmetry $Fm3m$) are given for Fe_2TiSn in Fig. 1. To explain the divergence between the shapes of the x-ray-diffraction lines (in the inset of Fig. 1) we calculated the x-ray-diffraction spectra for the monoclinic (symmetry $C2/c$) and orthorhombic (symmetry $F222$) structures. For Fe_2TiSn, the best fit for the monoclinic deformations of the $L2_1$ structure gives $a = 6.084$ Å, $b = 6.073$ Å, $c = 6.103$ Å, and $\beta = 89.43°$, while for the orthorhombic structure it gives $a = 6.025$ Å, $b = 5.98$ Å, and $c = 6.065$ Å. However, in both the cases there is not good agreement between the intensities of the x-ray-diffraction spectrum and the calculated intensities. This may be due to atomic disorder which can be caused by the following.

(1) Small off-stoichiometry grains (clusters) with slightly different lattice parameters than those of the homogeneous Fe_2TiSn compound may be distributed throughout the polycrystalline sample.

(2) Polycrystalline samples of the $Fe_2Ti_{1-x}V_xSn$ system can show a periodic segregation of Fe atoms formed by the alternation of enriched and depleted clusters aligned along some direction of the matrix. This periodic composition fluc-

TABLE I. Heusler alloys investigated and their structural and calculated magnetic properties. Calculated DOS at ϵ_F and the magnetic moment μ. (NM and FM symbols denote, respectively, the non-spin-polarized and spin-polarized mode of calculations.)

Compound	$Fm3m$ a in Å	DOS at ϵ_F (eV^{-1}/f.u.)	μ (μ_B/f.u.; μ_B/atom)
Fe_2TiSn	6.074	0.52 (LMTO)	0
		0.0 (LAPW LSDA, LSDA+U)	0
$Fe_{17}Ti_7Sn_8$	6.069	0.0 (LMTO)	0
$[Fe_{15}Ti_{AS}][Ti_7Fe_{AS}]Sn_8$	6.069	1.83 (LMTO-NM)	0
		2.12 (LMTO-FM)	0.49
$Fe_2Ti_{0.95}V_{0.05}Sn$	6.070	3.68 (KKR-CPA)	0
$Fe_2Ti_{0.875}V_{0.125}Sn$		2.79 (LMTO)	0
$Fe_2Ti_{0.8}V_{0.2}Sn$	6.065	3.63 (KKR-CPA)	0.52 Fe: 0.32 Ti: −0.13 V: 0 Sn: −0.02
$Fe_2Ti_{0.75}V_{0.25}Sn$		2.68 (LMTO)	0.23 Fe: 0.16 Ti: −0.09 V: −0.13 Sn: −0.02
$Fe_2Ti_{0.7}V_{0.3}Sn$	6.050	4.01 (KKR-CPA)	0.6 Fe: 0.37 Ti: −0.15 V: −0.06 Sn: 0.02
$Fe_2Ti_{0.6}V_{0.4}Sn$	6.038	4.42 (KKR-CPA)	0.67 Fe: 0.42 Ti: −0.17 V: −0.11 Sn: −0.03
$Fe_2Ti_{0.5}V_{0.5}Sn$	6.044	3.34 (LMTO)	0.43 Fe: 0.32 Ti: −0.16 V: −0.21 Sn: −0.02
Fe_2VSn	5.959 (Ref. 16)	4.34 (LMTO)	0.81 Fe: 0.62 V: −0.38 Sn: −0.04

tuation could be understood as the wavelength of the composition modulation. This modulated structure may be observed by the formation of satellite reflections around each x-ray-diffraction peak. This possibility is currently under investigation.

B. Electronic structure

Figures 2 and 3 show the band structure and the total DOS of the compound Fe_2TiSn. Apart from energies close to the Fermi energy (ε_F), band structure and total DOS calculations performed using various methods show almost the same shape, which is similar to that calculated for other transition metal nonmagnetic Heusler compounds.[9–11,32,33] The total DOS spectrum decomposes into three clearly separated parts. A band located in the binding energy (BE) range of 8–11 eV and separated by a gap of ~2 eV from the valence band originating from the *s* states of Sn. The *p* states of Sn hybridize with the *spd* states of TM (Fe, Ti) atoms to form a well resolved band visible in the BE range of 3–6 eV separated from the rest of valence band by a low-DOS dip. The part of the valence band which extends from 3 eV to ε_F is composed mainly of TM *d* states. The distribution of *d* states with different symmetries (e_g and t_{2g}) agrees with the scheme described by Galanakis *et al.*[15]. The states with e_g symmetry (of both TM atoms) dominate at the bottom edge of the valence band. According to the scheme of Galanakis *et al.*, the valence-band complex located at energies between 0.5 and 2 eV is formed mainly by the Fe-*d* states of t_{2g}

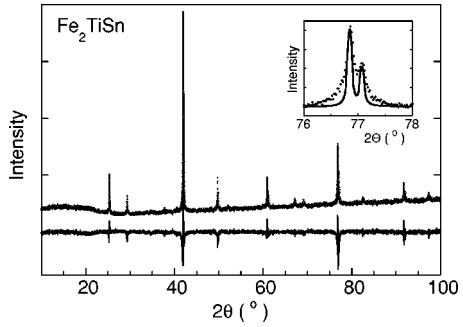

FIG. 1. The observed (points) and calculated (solid line) x-ray-diffraction pattern of the cubic Fe_2TiSn (space group $Fm3m$). The bottom is the difference between the observed and calculated intensities. Inset: an experimental and calculated profile of the (220) diffraction line.

character and can be decomposed into a low-energy band of t_{2g} states and states of t_{1u} symmetry located near the Fermi level. The conduction-band DOS starts just at ε_F [Fig. 3(a)] or above ε_F [Figs. 3(b) and 3(c)] and is separated from the valence band by a gap or quasigap. The *d* states of Fe with symmetry e_u form a flat band near the Fermi level [in Figs. 2(a) and 3(b)] and the related sharp rise and peak of the DOS above ε_F (shown in Fig. 3). The unoccupied e_g and t_{2g} bands of the Ti-*d* states follow in agreement with the scheme of Galanakis *et al.*[15]

The shape of the DOS generally does not depend on the method used for the calculations, excluding the narrow range of energies in the vicinity of ε_F. The DOS obtained by the TB-LMTO method displays a deep quasigap with the Fermi

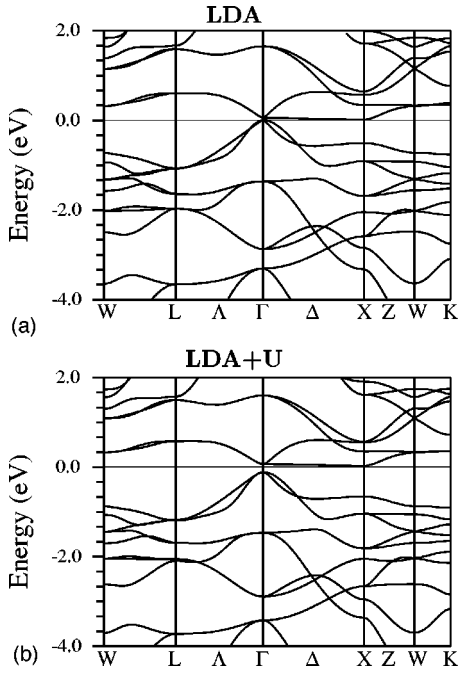

FIG. 2. FP-LAPW band structure of Fe_2TiSn with (a) LDA and (b) LDA+U exchange-correlation potential along various symmetry directions in the Brillouin zone. The zero of the energy scale is shifted to the Fermi energy.

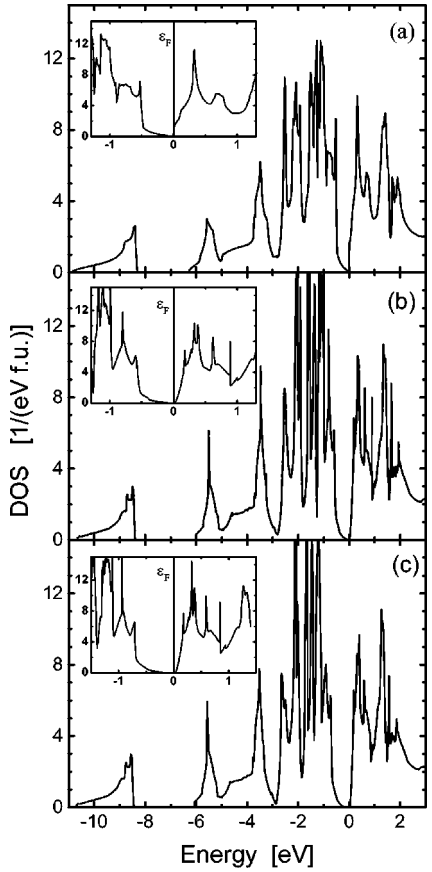

FIG. 3. The total density of states (DOS) calculated for Fe_2TiSn with the use of three different approaches: (a) TB-LMTO; (b) FP-LAPW LDA; (c) FP-LAPW LDA+U. The zero of the energy scale is positioned at the Fermi energy. Insets show the total DOS in the vicinity of Fermi level.

energy located at the bottom edge of the conduction band [Fig. 2(a)], while the FP-LAPW with the use of both the LSDA and LSDA+U XC potentials shows the direct energy gap located just at ε_F. The minimal width of the gap (at the Γ $\vec{k}$ point) obtained with the use of LSDA XC potential is 0.013 eV. It increases ten times when the LDA+U correction is taken into account.

In Fig. 4, we present numerical calculations of the electronic density of states (TB-LMTO DOS) of Fe_2TiSn. Also shown in the figure, for comparison, are the XPS valence-band spectra. The well-defined peaks in the XPS spectra are due to electrons which have not suffered an inelastic energy loss emerging from the sample. Electrons that have lost energy increase the level of the background at binding energies higher than the peak energy. All XPS bands have had their backgrounds subtracted which were calculated by means of the Tougaard algorithm.[34] The XPS peak intensity also depends on the photoelectronic cross section for the atomic orbital of interest. To obtain better agreement between the calculated spectra and the experimentally obtained one, the shapes of the DOS are convoluted with Lorentzians with half width equal to 0.4 eV and the proper cross sections for partial states on each atom of the unit cell, which are taken from Ref. 35. The width of the Lorentzian (0.4 eV) was assumed

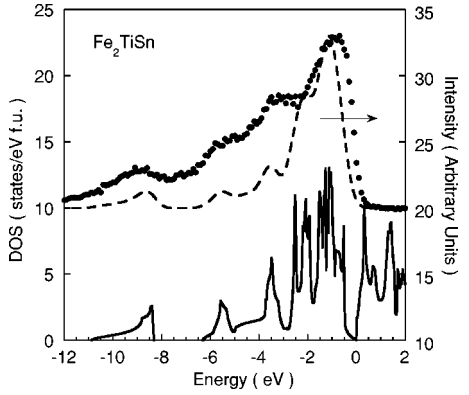

FIG. 4. The total DOS of the cubic ($Fm3m$) Fe_2TiSn (thin curve), convoluted with Lorentzians of half width 0.4 eV, taking into account proper cross sections for bands with different l symmetry (dotted curve), is compared to the measured XPS valence-band data corrected for background (points).

to be equal to instrumental broadening. The energy spectra of the electrons were analyzed with an energy resolution better than 0.4 eV. The experimental spectra are qualitatively very similar to the approximated DOS curves. In Table I the DOS at ϵ_F are listed along with the calculated magnetic moments μ obtained for $Fe_2Ti_{1-x}V_xSn$ by TB-LMTO or KKR-CPA. As one adds V, the magnetic moment gradually increases, and reaches the maximal value for Fe_2VSn (Table I); however, the values of μ obtained from the disordered KKR-CPA method are always higher than those obtained from the ordered TB-LMTO. This result may be a consequence of atomic disorder which usually increases the calculated value of μ in KKR-CPA. It may also be due to the different approximations used for the XC potential in both methods.

Results of TB-LMTO band-structure calculations for off-stoichiometric $Fe_{17}Ti_7Sn_8$ and defected $[Fe_{15}Ti_{AS}]\times[Ti_7Fe_{AS}]Sn_8$ structures are presented in Figs. 5 and 6, respectively. For the $Fe_{17}Ti_7Sn_8$ off-stoichiometric composition only the nonmagnetic solution has been found. In $Fe_{17}Ti_7Sn_8$, an excess of Fe_{AS} atoms at V antisite positions leads to the creation of a sharp and narrow peak in the DOS below ε_F (Fig. 5) and in the middle of energy gap observed in the stoichiometric Fe_2TiSn compound (Fig. 3). The DOS of this peak is composed mainly of the $d-e_g$ states of Fe_{AS} which hybridize with the d states of the eight nearest Fe atoms in octahedral coordination. The contribution to the DOS peak by other TM atoms (Fe and Ti), which are more distant from the Fe_{AS} defect, is negligible. The ε_F located above the peak falls into the true energy gap of 0.06 eV.

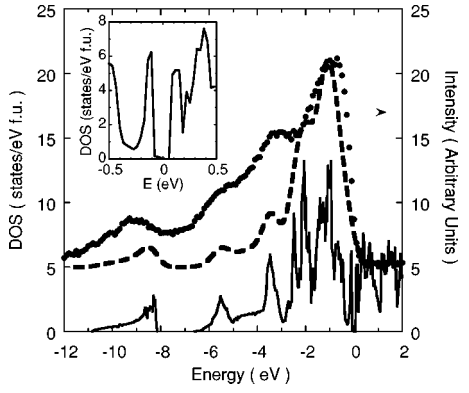

FIG. 5. Numerical calculations of the total DOS of paramagnetic $Fe_{17}Ti_7Sn_8$ (space group: $Fm3m$, the supercell contains eight unit cells). The total DOS (thin curve), convoluted with Lorentzians of half width 0.4 eV, taking into account proper cross sections for bands with different l symmetry (dotted curve), compared to the measured XPS valence-band data obtained for $Fe_{21}Ti_9Sn_{10}$, corrected for background (points). Inset: expanded DOS plot near ϵ_F for $Fe_{17}Ti_7Sn_8$.

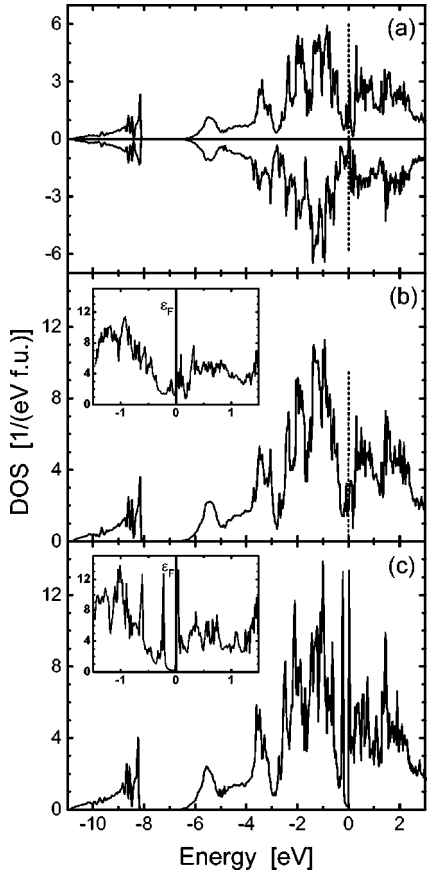

FIG. 6. The total density of states (DOS) calculated for the $[Fe_{15}Ti_{AS}][Ti_7Fe_{AS}]Sn_8$ supercell. Part (a) shows the spin-resolved total DOS with majority-spin DOS placed at the bottom panel. Part (b) gives the total DOS resulting from the spin-polarized (FM) calculations. In part (c), the DOS resulting from the nonspin-polarized is shown. (The zero of the energy scale is positioned at the Fermi energy marked by dash lines at part (a) and (b). Insets show the total DOS in the vicinity of the Fermi level.)

For an $[Fe_{15}Ti_{AS}][Ti_7Fe_{AS}]Sn_8$ alloy with structural defects, both magnetic and nonmagnetic solutions have been found within the TB-LMTO approach. The spin resolved and the total DOS for the magnetic solution are presented in Figs. 6(a) and 6(b), respectively.

The DOS of $[Fe_{15}Ti_{AS}][Ti_7Fe_{AS}]Sn_8$ in the magnetic state exhibits a half metallic character at the Fermi level, i.e., the minority-spin states contribute to the DOS (ε_F), while the majority-spin DOS forms a narrow quasigap at ε_F (Fig. 6). Apart from some features visible within the energy range of

$\varepsilon_F \pm 0.5$ eV, the shape of the total DOS (with three well separated subbands) resembles that of the pure Heusler compound Fe_2TiSn (in Fig. 3), in both the magnetic and nonmagnetic [Fig. 6(c)] states.

Shown in Fig. 5 is a comparison of the calculated DOS of $Fe_{17}Ti_7Sn_8$ and the XPS spectra for $Fe_{21}Ti_9Sn_{10}$. The LMTO calculations predicted a nonmagnetic ground state for this material as well as an interesting electronic structure in the DOS near ϵ_F. There is also an energy gap and a sharp peak in the *d* states located ~ 0.1 eV below ϵ_F. The XPS resolution is not good enough to see any structure in the XPS spectra near ϵ_F. Hence, it is not possible to confirm the band-structure calculations for the extra *d* peak in the gap for the off-stoichiometric material. However, in accord with band-structure calculations near the Fermi level, an infrared study performed on Fe_2TiSn (Ref. 13) suggests that there are additional bands centered near ϵ_F and an interband transition which can be interpreted as excitation across a pseudogap.

The two magnetic and nonmagnetic solutions calculated for the $[Fe_{15}Ti_{AS}][Ti_7Fe_{AS}]Sn_8$ composition are found very close on the total-energy scale. The magnetic energy gain upon magnetic polarization is ~ 520 K/f.u. ($=130$ K/atom) which relates to the magnetic critical temperatures observed in these materials. The calculated magnetic structure of $[Fe_{15}Ti_{AS}][Ti_7Fe_{AS}]Sn_8$ is of cluster character. The magnetic properties of this sample are attributed to the Fe_{AS} atomic defects with a localized magnetic moment of $2.67\mu_B$. In the nearest neighborhood of Fe_{AS}, the magnetic moment localized on the remaining seven Fe atoms is only $0.2–0.4\mu_B$, while the Ti_{AS} atom shows opposite induced polarization with a local moment of $0.4\mu_B$. The cluster consists of Fe_{AS} and eight surrounding atoms ($7\times Fe + Ti_{AS}$) and shows an effective moment of $\sim 4.5\mu_B$. These magnetic clusters, located at every eighth unit cell, are embedded in an oppositely polarized background of Sn atoms and TM (Fe, Ti) atoms located at second and next coordination spheres of Fe_{AS} magnetic defects.

X-ray-diffraction analysis of Fe_2TiSn suggests that there is a monoclinic or orthorhombic deformation of the $L2_1$ cubic structure. Based on this we analyzed the electronic structure of the orthorhombic Fe_2TiSn alloy (space group: $F222$, lattice parameters listed in Table I) using the LSDA FP-LAPW method. The results of these calculations are only slightly changed in comparison to the results obtained for the cubic alloy. The electronic structure calculations for the orthorhombic distortion, using the PBE XC-potential, predict a nonmagnetic solution with ~ 5 mRy higher total energy of the crystal in comparison to that of cubic Fe_2TiSn with the $L2_1$-type structure.

Figures 7 and 8 show the DOS calculated for $Fe_2Ti_{0.8}V_{0.2}Sn$ by KKR-CPA and TB-LMTO and for $Fe_2Ti_{0.5}V_{0.5}Sn$ by TB-LMTO. The calculated XPS spectra are compared to the experimental XPS spectra. Both methods give a magnetic ground state for $Fe_2Ti_{1-x}V_xSn$ alloys with $x \geqslant 0.2$. In TB-LMTO calculations the exchange splitting reduces the gap (or pseudogap) at ϵ_F. Atomic disorder in KKR-CPA clearly suppresses the gap, and as a result, the DOS near ϵ_F displays a deep valley. In general, there is a good agreement between the XPS spectra obtained experimentally and the calculated ones. However, in the vicinity of ϵ_F, the TB-LMTO calculations are in much better agreement with experiment.

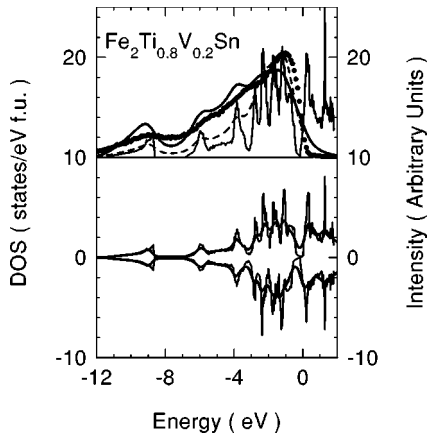

FIG. 7. Numerical calculations of the DOS of $Fe_2Ti_{0.75}V_{0.25}Sn$ for both spin directions (TB-LMTO—thin line and SPR-KKR—thick line). The upper panel shows the total TB-LMTO DOS of the cubic ($Fm3m$) $Fe_2Ti_{0.75}V_{0.25}Sn$ (thin curve). The DOS convoluted with Lorentzians of half width 0.4 eV, taking into account proper cross sections for bands with different *l* symmetry (dotted curve), compared to the measured XPS valence-band data for the $Fe_2Ti_{0.8}V_{0.2}Sn$ sample, corrected for background (points). The thick line represents the simulated XPS spectrum obtained from SPR-KKR calculations. The measured XPS spectra and the calculated XPS spectra are plotted in the upper figure in arbitrary units.

C. Magnetic susceptibility

Shown in Fig. 9 are magnetic susceptibility χ data plotted as χ versus T and χ^{-1} versus T between 1.8 and 300 K for $Fe_2Ti_{1-x}V_xSn$ alloys. The magnetic susceptibility χ deviates

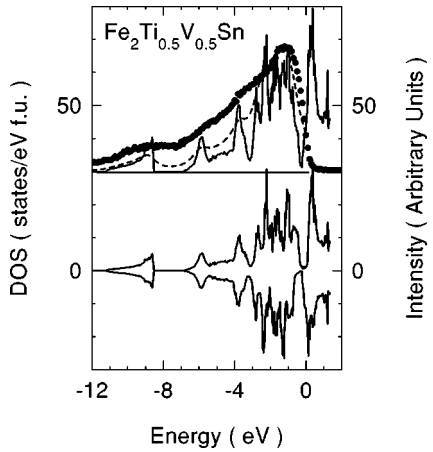

FIG. 8. Numerical calculations of the DOS of $Fe_2Ti_{0.5}V_{0.5}Sn$ for both spin directions. The total DOS (thin curve), convoluted with Lorentzians of half width 0.4 eV, taking into account proper cross sections for bands with different *l* symmetry (dotted curve), is compared to the measured XPS valence-band data, corrected for background (points). The measured XPS valence-band data and the calculated XPS spectra are plotted in the upper panel in arbitrary units.

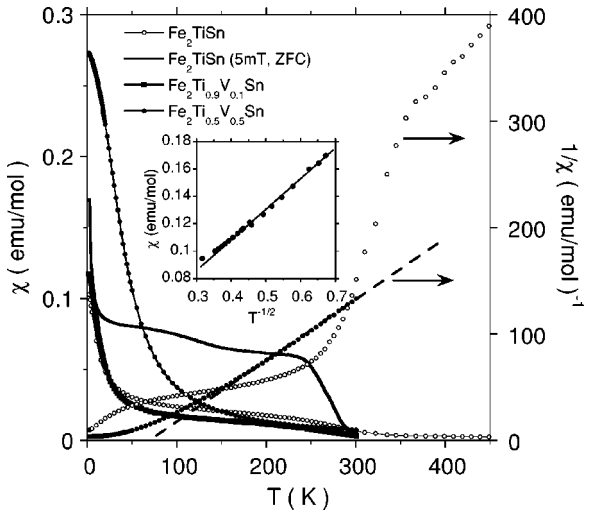

FIG. 9. Magnetic susceptibility χ and χ^{-1} vs temperature for Fe_2TiSn, $Fe_2Ti_{0.9}V_{0.1}Sn$, and $Fe_2Ti_{0.5}V_{0.5}Sn$. The applied magnetic field was 0.5 T. For Fe_2TiSn, the ZFC susceptibility was also measured at a magnetic field of 5 mT (solid curve). The inset shows the ZFC χ measured at $H=5$ mT for Fe_2TiSn vs $T^{-1/2}$.

markedly from a Curie-Weiss law for Fe_2TiSn and $Fe_2Ti_{0.9}V_{0.1}Sn$ and signals the onset of the weak magnetic behavior. Some rather characteristic features in $\chi(T)$ coincide with an abnormal change visible at ~ 240 K in the experimental lattice parameter a versus T plot (in Fig. 10). In Ref. 7 the magnetic-susceptibility anomaly was found to arise from a distribution of magnetic defects. While Fe_2TiSn is nominally nonmagnetic, magnetization can be induced in this alloy by wrong site iron atoms as a result of incomplete ordering.[36] Recently we attributed this abnormal change of χ at ~ 240 K to thermal fluctuations of ferromagnetic Fe particles induced by atomic disorder.[37] Since χ versus T curves exhibit very similar features in the Ti-rich $Fe_2Ti_{1-x}V_xSn$ alloys, one explanation for enhanced susceptibility $\chi(T)$ below room temperature is the presence of superparamagnetism in the $Fe_2Ti_{1.9}V_{0.1}Sn$ sample.

The susceptibility data also show that χ under zero-field cooling (ZFC) is linear with $T^{-1/2}$ for $Fe_2Ti_{1.9}V_{0.1}Sn$ (inset of Fig. 9) at $T<9.5$ K. Anderson[38] showed that if spin compensation is the dominant mechanism responsible for the low-temperature magnetic behavior, χ varies as $T^{-1/2}$ in the low-temperature limit; the ZFC χ versus T data are in good agreement with this theoretical prediction and indicate Kondo-lattice behavior.

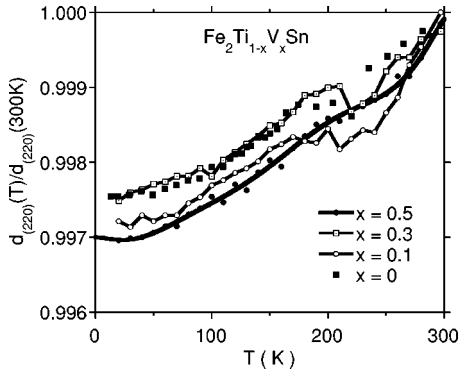

FIG. 10. The distance between two (220) crystallographic planes d_{220} normalized to d_{220} at $T=300$ K vs temperature for $Fe_2Ti_{1-x}V_xSn$ alloys.

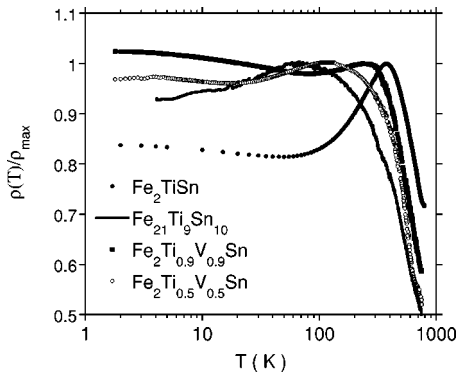

FIG. 11. Reduced electrical resistivity $\rho(T)/\rho_{max}$ vs $\ln T$ for Fe_2TiSn, $Fe_{21}Ti_9Sn_{10}$, $Fe_2Ti_{0.9}V_{0.1}Sn$, and $Fe_2Ti_{0.5}V_{0.5}Sn$. The values of ρ at T_{max} are, respectively: 487 $\mu\Omega$ cm ($T_{max}=376$ K) for Fe_2TiSn, 549 $\mu\Omega$ cm ($T_{max}=64.8$ K) for $Fe_{21}Ti_9Sn_{10}$, 991 $\mu\Omega$ cm ($T_{max}=246$ K) for $Fe_2Ti_{0.9}V_{0.1}Sn$, and 371 $\mu\Omega$ cm ($T_{max}=120$ K) for $Fe_2Ti_{0.5}V_{0.5}Sn$.

However, the susceptibility data plotted in Fig. 9 show that $\chi(T)$ obeys the Curie-Weiss law for $Fe_2Ti_{0.5}V_{0.5}Sn$ at $T>40$ K. The fit parameters to the equation $\chi(T)=C/(T-\theta)+\chi_0$ are $C=2.90$ emuK/mol, $\theta=20.5$ K, and $\chi_0=1\times10^{-3}$ emu/mol. The constant $C=N\mu^2/3k_B$ has a value that is close to the value C expected for an iron configuration d^6Fe^{2+}, if one assumes that the angular momentum of the Fe ions is quenched in the disordered alloy, i.e., $J=S$ and $g_J=2$.

The LMTO calculations for $Fe_2Ti_{0.5}V_{0.5}Sn$ predicted a magnetic ground state (Table I) with a magnetic moment of $0.43\mu_B$ per formula unit which is comparable to the saturation magnetic moment μ obtained from an extrapolation of the M versus $1/H$ plots to $1/H=0$.

The magnetic properties are enhanced with increasing V concentration in $Fe_2Ti_{1-x}V_xSn$. Fe_2VSn is known to be a ferromagnet with a Curie temperature $T_C=200$ K and $\mu=1.32$ μ_B per formula unit.[16] Our LMTO calculations predict a magnetic moment $\mu=0.81\mu_B$ for Fe_2VSn which is smaller than the value obtained experimentally. This disagreement can result from atomic disorder, obtained experimentally for the Fe-Heusler alloys, which leads to strong enhancement of the magnetic moment.[7]

D. Electrical resistivity

Shown in Fig. 11 are electrical resistivity ρ/ρ_{max} versus T data for $Fe_2Ti_{1-x}V_xSn$ and $Fe_{21}Ti_9Sn_{10}$ between 1.8 and 750 K, where ρ_{max} is the maximal value of ρ for each curve which is located at 377 K for Fe_2TiSn, 230 K for $Fe_2Ti_{0.9}V_{0.1}Sn$, and 112 K for $Fe_2Ti_{0.5}V_{0.5}Sn$. The resistivity minimum in $\rho(T)$ is strongly reduced with applied magnetic field (Fig. 12). The negative magnetoresistance for $Fe_2Ti_{0.9}V_{0.1}Sn$, which at $T=1.8$ K is about 7% of the resis-

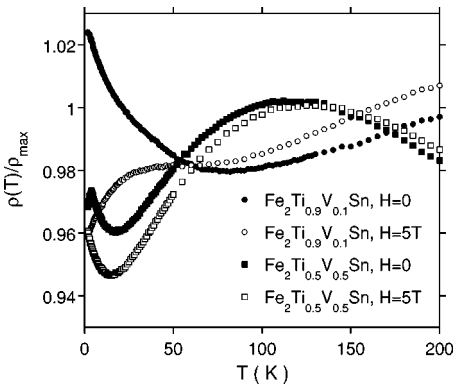

FIG. 12. Reduced electrical resistivity $\rho(T)/\rho_{max}$ vs T for $Fe_2Ti_{0.9}V_{0.1}Sn$ and $Fe_2Ti_{0.5}V_{0.5}Sn$, measured at $H=0$ and at $H=5$ T (open points).

tivity value at $H=0$, is a characteristic of Kondo-lattice compounds. The resistivity data presented in Fig. 12 also provide further evidence for Kondo-lattice behavior in $Fe_2Ti_{1-x}V_xSn$. One can distinguish Fe_2TiSn and $Fe_2Ti_{0.9}V_{0.1}Sn$, both of which have a $\ln T$ dependence of ρ and $Fe_2Ti_{0.5}V_{0.5}Sn$ which had $\ln T$ and a sharp peak in ρ at $T=4.1$ K, resulting from the magnetic phase transition. In this alloy, we suggest a magnetic ground state in a Kondo lattice with partial screening. The resistivity at T_{max} is 490 $\mu\Omega$cm for Fe_2TiSn, 580 $\mu\Omega$cm for $Fe_{21}Ti_9Sn_{10}$, and 950 $\mu\Omega$cm for $Fe_2Ti_{0.9}V_{0.1}Sn$, while for the magnetic $Fe_2Ti_{0.5}V_{0.5}Sn$ sample, $\rho_{max}=370$ $\mu\Omega$ cm. Upon increasing the temperature, ρ decreases smoothly and at 750 K reaches a value within the range 73–50 % of ρ_{max}. Our ρ data cannot be described by a hopping-type temperature dependence[39] where $\rho=\rho_0\exp(T_0/T)^p$ but rather by a two-level Schottky function $\rho=a+b(T_0/T)^2\exp(T_0/T)/[1+\exp(T_0/T)]^2$. For Fe_2TiSn, the fit parameter is $T_0=800$ K. The divergence between the experimental data and the calculated curve is too high, especially at temperatures $T<T_{max}$. We can only speculate that the mechanism causing the observed electrical transport properties could be attributed to interband transitions through a small gap located at ϵ_F and is roughly understood in terms of thermal excitations (i.e., a many-body problem).

E. Many-body aspects

An additional aim of this investigation of $Fe_2Ti_{1-x}V_xSn$ was to calculate, within the many-electron model, the temperature variation of the quasiparticle structure and the measured quantities like electrical resistivity, thermoelectric power, electronic specific heat, etc. From the band-structure calculations presented for defected $Fe_{17}Ti_7Sn_8$ and $[Fe_{15}Ti_{AS}][Ti_7Fe_{AS}]Sn_8$ structures it becomes clear that the sharp DOS feature visible just below ε_F is due to the $d-e_g$ (e_u) states of Fe_{AS} atoms.[15] The doubly degenerate Fe_{AS} $d-e_g$ band is almost fully occupied. The electrons of that band (denoted in the following as d electrons) propagate by first forming a d hole which interacts with the other electrons from much broader bands. The accompanying dynamical processes are discussed in detail in Ref. 40.

Taking into account the analysis of the one-particle electronic structure, we started the many-body investigation along the line described by Liu.[41] The proposed two-band Hamiltonian with a strongly correlated, narrow band interacting via hybridization with a broad band was applied to describe the non-Fermi-liquid behavior of the cerium and uranium compounds.[41] The similarity of the physical properties and the single-particle electronic structure of $Fe_2Ti_{1-x}V_xSn$ with those of cerium and uranium compounds[42,43] supports the supposition that the origin of the physical properties of both groups of materials is the same.

Therefore, to investigate thermodynamic properties of $Fe_2Ti_{1-x}V_xSn$ alloys we consider a Hamiltonian which is a version of the Kimball-Falicov model[41]

$$H=\sum_{\mathbf{k}\sigma}\varepsilon_{\mathbf{k}}^{(c)}c_{\mathbf{k}\sigma}^{\dagger}c_{\mathbf{k}\sigma}+\sum_{i,\sigma}\varepsilon_i^{(d)}d_{i\sigma}^{\dagger}d_{i\sigma}$$
$$-U_{cd}\sum_{i,\sigma\sigma'}\sum_{\mathbf{k},\mathbf{k}'}d_{i\sigma}d_{i\sigma}^{\dagger}c_{\mathbf{k}\sigma'}^{\dagger}c_{\mathbf{k}'\sigma'}e^{i(\mathbf{k}-\mathbf{k}')\mathbf{R}_i}$$
$$+V\sum_{i\mathbf{k}\sigma}(c_{\mathbf{k}\sigma}^{\dagger}d_{i\sigma}e^{-i\mathbf{k}\mathbf{R}_i}+\text{H.c.})+U_{dd}\sum_i d_{i\uparrow}^{\dagger}d_{i\uparrow}d_{i\downarrow}^{\dagger}d_{i\downarrow}, \quad (1)$$

where the first term represents the kinetic energy of the conduction (c) electrons. The second term stands for the energy of electrons in the localized orbitals of the narrow Fe_{AS} $d-e_g$ band. The U_{cd} term represents the Coulomb attraction between the $d-e_g$ hole and quasi-free band electron. The V term is the c-d hybridization which is assumed to be weak, and the last term (U_{dd}) describes the Coulomb repulsion within the d band.

The approximations used in the Hamiltonian equation (1) are made within the scheme which provides the following simple physical picture. It is assumed that the heavy d electron propagates via hybridization with a broad band of c electrons. The process involves the hopping of the d electron in and out of the Fe_{AS} site. The Fe_{AS} narrow energy band lies inside the broad c band. The creation of the d hole gives rise to a strong local attractive potential to the c band electrons represented in the Hamiltonian equation (1) by U_{cd}. The hopping of the hole generated in this way is accompanied by a simultaneous motion of the charge cloud. Such an oscillating cloud is represented in the model by a local harmonic oscillator (local boson) which can be excited to higher energies with increasing temperature T. The characteristic oscillator frequency ω_0 after some standard manipulations was included in the model parameters. Following Ref. 41, we also ignore the effect of Coulomb repulsion U_{ff} in zeroth order and restrict the occupation number of the d band to less than one. The propagation of the d electron within the crystal is similar to that of a polaron in insulators.

The derivation of the Dyson equation for the *d* electrons is complicated and tedious and the interesting details can be found in Ref. 41. The final form of the equation used is

$$\omega-\varepsilon_{\mathbf{k}}^{(c)}=\frac{W}{4\Gamma(\alpha)}\left[\frac{\beta}{\pi}\right]^{\alpha-1}\frac{e^{\beta x}+e^{-i\pi\alpha}}{\cosh(\beta x)+\cos(\pi\alpha)} \times\int_0^{\beta}e^{-\tau x}\left[\sin\left(\frac{\pi\tau}{\beta}\right)\right]^{\alpha-1}\mathrm{d}\tau, \quad (2)$$

where $\beta=(k_{\mathrm{B}}T)^{-1}$, $x=(\omega-\varepsilon^d)/\eta$.

The energy parameter $\eta(=[2\pi V^2 A\csc(\pi\alpha)/W]^{1/\alpha})$ determines the characteristic energy scale of the model and depends on the interaction strengths V, U_{cd} ($\alpha\propto U_{cd}$), Γ is the Euler gamma function and W is the *c*-band width. In the investigations presented here the *c*-electron Bloch-DOS was used in the form of a wide parabola simulating the Fe_2TiSn-DOS near ε_F (Fig. 3). The position of the atomic *d* level was assumed to be $\varepsilon^d=0$ and the *c*-*d* hybridization constant $V=0.1$ eV was established. The value of α was taken to be close to 1.0.[41] For the calculations of the resistivity, we used the Boltzmann-like formula given in Ref. 41. The Dyson equation for the self-energy, which describes the quasiparticles in the *d* band, was solved numerically. Because of the very flat *c* band the *d* electrons play an essential role in creating quasiparticles. The structure of the resulting quasiparticle spectrum is temperature dependent.

The concept of the Dingle temperature[41] (T_D) was used to simulate broadening of the DOS peak visible at ε_F [Fig. 13(c)] for increasing concentration of the Fe_{AS} atoms. Doniach and Sunjic[44] studied the x-ray edge problem at $T=0$ K for disordered systems and observed broadening of the singularity in a way similar to that of increasing temperature.

Figure 13(b) presents the results for the resistivity. The calculated temperature and disorder dependencies of the resistivity follow qualitatively the experimental observations.

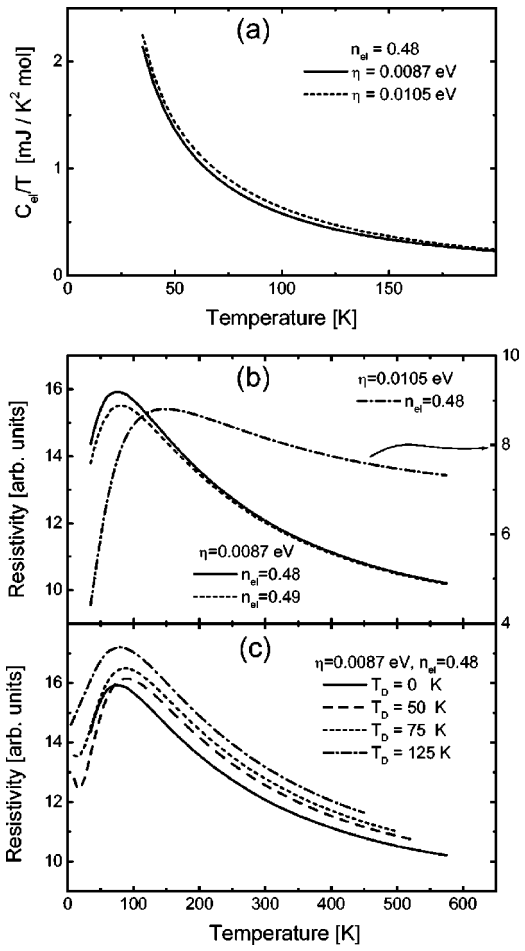

FIG. 13. The temperature dependence of (a) the *d*-like quasiparticle specific heat C_{el} divided by temperature *T*, (b) the *d*-like quasiparticle electrical resistivity for different sets of model parameters η and *d*-like quasiparticle band populations n_{el}, and (c) the *d*-like quasiparticle electrical resistivity for different degrees of atomic disorder simulated by a Dingle temperature.

IV. SUMMARY

Experimental investigations have shown that several properties observed in the Fe_2TiSn Heusler alloy, e.g., the semiconductor-like behavior of the resistivity, the large (compared to a normal metal) value of the low-temperature electronic specific-heat coefficient, and the low-temperature magnetic susceptibility $\chi\sim T^{-1/2}$, resemble those observed in the nonmagnetic narrow-gap semiconductor FeSi known as a *d* Kondo insulator. The Fe_2TiSn crystallizes in the $L2_1$ structure; however, a more detailed analysis of the x-ray-diffraction data suggests a modulated structure or orthorhombic distortion of the unit cell, both cases resulting from atomic disorder.

The electronic structure calculations have shown that Fe_2TiSn is semimetallic and nonmagnetic. The TB-LMTO method proved that the Fe defects in the nonmagnetic system give rise to a narrow, and strongly correlated *d*-like band located in the energy gap near ϵ_F. For the $Fe_2Ti_{1-x}Fe_xSn$ and $Fe_2Ti_{1-x}V_xSn$ alloys, where $x\leqslant 0.1$, the band-structure calculations also predict a nonmagnetic ground state; however, atomic disorder leads to the appearance of a magnetic cluster. Using the TB-LMTO method, we have shown that for $[Fe_{15}Ti_{AS}][Ti_7Fe_{AS}]Sn_8$ with a small concentration of Fe_{AS} atoms at antisite positions, the calculations predict a flat, narrow band (narrow peak in DOS) located just below ϵ_F, which results from the hybridized *d* states of the cluster. The narrow peak in the DOS attributed to Fe_{AS} occupying antisite atomic positions leads to anomalous thermodynamic properties in Fe_2TiSn and its V alloys attributed to many-body effects. The high-temperature resistivity data obtained for Fe_2TiSn, $Fe_{21}Ti_9Sn_{10}$, $Fe_2Ti_{0.9}V_{0.1}Sn$, and $Fe_2Ti_{0.5}V_{0.5}Sn$ suggest that the mechanism of the electrical transport properties are attributed to interband transitions through a small gap located at ϵ_F, in agreement with our numerical calculations. Therefore, during our investigation of the thermodynamic properties of $Fe_2Ti_{1-x}V_xSn$ alloys, we considered the Kimball-Falicov model, which qualitatively describes the experimental $\rho(T)$ dependencies. The Dingle temperature was used to simulate broadening of the DOS peak visible at ϵ_F.

The electronic structure of the $Fe_2Ti_{1-x}V_xSn$ alloys are

also investigated by KKR-CPA method to analyze the influence of atomic disorder on electronic and magnetic properties of these alloys. Both TB-LMTO and KKR-CPA numerical calculations yield a magnetic ground state for $Fe_2Ti_{1-x}V_xSn$ alloys when $x \geqslant 0.2$; they also give an increase of magnetic moment as a function of V concentration.

ACKNOWLEDGMENTS

This work was partly supported by the Center of Excellence for Magnetic and Molecular Materials for Future Electronics within the European Commission Contract No. G5MA-CT-2002-04049.

[1] F. Heusler, Verh. Dtsch. Phys. Ges. **5**, 219 (1903).
[2] P.J. Webster and K.R.A. Ziebeck, in *Magnetic Properties of Metals*, edited by H.P.J. Wijn, Landolt-Börnstein, New Series 1, Group III, Vol. 19c (Springer, Berlin, 1988), p. 75.
[3] K.R.A. Ziebeck and K.-U. Neumann, in *Magnetic Properties of Metals*, edited by H.P.J. Wijn, Landolt-Börnstein, New Series 1, Group III, Vol. 32c (Springer, Berlin, 2001), p. 64.
[4] J. Kübler, A.R. Williams, and C.B. Sommers, Phys. Rev. B **28**, 1745 (1983).
[5] K.R.A. Ziebeck and P.J. Webster, J. Phys. Chem. Solids **35**, 1 (1974).
[6] J. Pierre, R.V. Skolozdra, Yu.K. Gorolenko, and M. Kouacou, J. Magn. Magn. Mater. **134**, 95 (1995).
[7] A. Ślebarski, M.B. Maple, E.J. Freeman, C. Sirvent, D. Tworuszka, M. Orzechowska, A. Wrona, A. Jezierski, S. Chiuzbaian, and M. Neumann, Phys. Rev. B **62**, 3296 (2000).
[8] Y. Nishino, M. Kato, S. Asano, K. Soda, M. Hayasaki, and U. Mizutami, Phys. Rev. Lett. **79**, 1909 (1997).
[9] R. Weht and W.E. Pickett, Phys. Rev. B **58**, 6855 (1998).
[10] D.J. Singh and I.I. Mazin, Phys. Rev. B **57**, 14 352 (1998).
[11] M. Weinert and R.E. Watson, Phys. Rev. B **58**, 9732 (1998).
[12] H. Okamura, J. Kawahara, T. Nanba, S. Kimura, K. Soda, U. Mizutani, Y. Nishino, M. Kato, I. Shimoyama, H. Miura, K. Fukui, K. Nakagawa, H. Nakagawa, and T. Kinoshita, Phys. Rev. Lett. **84**, 3674 (2000).
[13] S.V. Dordevic, D.N. Basov, A. Ślebarski, M.B. Maple, and L. Degiorgi, Phys. Rev. B **66**, 075122 (2002).
[14] J. Kübler, Physica B **127**, 257 (1984).
[15] I. Galanakis, P.H. Dederichs, and N. Papanikolau, Phys. Rev. B **66**, 174429 (2002).
[16] P.G. Engen, K.H.J. Buschow, and M. Erman, J. Magn. Magn. Mater. **30**, 374 (1983); K.H.J. Buschow, P.G. van Engen, and R. Jongebreur, *ibid.* **38**, 1 (1983).
[17] Y. Baer, G. Busch, and P. Cohn, Rev. Sci. Instrum. **46**, 466 (1975).
[18] O.K. Andersen and O. Jepsen, Phys. Rev. Lett. **53**, 2571 (1984); O.K. Andersen, O. Jepsen, and M. Sob, in *Electronic Structure and Its Applications*, edited by M. Yussouff (Springer, Berlin, 1987), p. 2.
[19] P. Blaha, K. Schwarz, G.K.H. Madsen, D. Kvasnicka, and J. Luitz, *WIEN2k, An Augmented Plane Wave + Local Orbitals Program for Calculating Crystal Properties* (Karlheinz Schwarz, Techn. Universitt Wien, Austria, 2001).
[20] O.K. Andersen and O. Jepsen, Physica B & C **91**, 317 (1977).
[21] U. von Barth and L. Hedin, J. Phys. C **5**, 1629 (1972).
[22] C.D. Hu and D.C. Langreth, Phys. Scr. **32**, 391 (1985).
[23] J.P. Perdew, K. Burke, and M. Ernzerhof, Phys. Rev. Lett. **77**, 3865 (1996).
[24] V.I. Anisimov, J. Zaanen, and O.K. Andersen, Phys. Rev. B **44**, 943 (1991); V.I. Anisimov, F. Aryasetiawan, and A.I. Lichtenstein, J. Phys.: Condens. Matter **9**, 767 (1997).
[25] M.M. Steiner, R.C. Albers, and L.J. Sham, Phys. Rev. B **45**, 13 272 (1992).
[26] D.J. Singh, Phys. Rev. B **44**, 7451 (1991).
[27] H. Ebert, P. Strange, and B.L. Gyorffy, J. Phys. F: Met. Phys. **18**, L135 (1988).
[28] H. Shiba, Prog. Theor. Phys. **46**, 77 (1971).
[29] A. Gonis, *Green Functions for Ordered and Disordered Systems* (North-Holland, Amsterdam, 1992).
[30] S.H. Vosko, L. Wilk, and M. Nussair, Can. J. Phys. **58**, 1200 (1980).
[31] H. Ebert, *Electronic Structure and Physical Properties of Solids*, Lecture Notes in Physics, edited by H. Dreysse, Vol. 335 (Springer, Berlin, 2000), p. 191 (the Münich SPR-KKR package, version 2.1; H. Ebert *et al.*, http://olymp.cup.uni-muenchen.de/ak/ebert/SPRKKR).
[32] A. Bansil, S. Kaprzyk, P.E. Mijnarends, and J. Tobola, Phys. Rev. B **60**, 13 396 (1999).
[33] J. Deniszczyk, Acta Phys. Pol. B **32**, 529 (2001).
[34] S. Tougaard and p. Sigmund, Phys. Rev. B **25**, 4452 (1982).
[35] J.J. Yeh and I. Lindau, At. Data Nucl. Data Tables **32**, 1 (1985).
[36] A. Jezierski and A. Ślebarski, J. Magn. Magn. Mater. **223**, 33 (2001).
[37] A. Ślebarski, M.B. Maple, A. Wrona, and A. Winiarska, Phys. Rev. B **63**, 214416 (2001).
[38] P.W. Anderson, Phys. Rev. **164**, 352 (1967).
[39] B.I. Shklovskii and A.L. Efros, *Electronic Properties of Doped Semiconductors* (Springer-Verlag, Berlin, 1984).
[40] G.D. Mahan, Phys. Rev. **163**, 612 (1967); P.W. Anderson, Phys. Rev. Lett. **18**, 1049 (1967); P. Nozières and C.T. De Dominicis, Phys. Rev. **178**, 1097 (1969).
[41] S.H. Liu, Physica B **240**, 49 (1997).
[42] A. Ślebarski, A. Jezierski, A. Zygmunt, S. Mähl, and M. Neumann, Phys. Rev. **58**, 13 498 (1998).
[43] A.I. Goldman, G. Shirane, G. Aeppli, B. Batlogg, and E. Bucher, Phys. Rev. B **34**, 6564 (1986).
[44] S. Doniach and M. Sunjic, J. Phys. C **3**, 285 (1970).